Exp Fluids (2012) 52:1533–1546
DOI 10.1007/s00348-012-1263-y

RESEARCH ARTICLE

# Flow control over a NACA 0012 airfoil using dielectric-barrier-discharge plasma actuator with a Gurney flap

**Li-Hao Feng · Timothy N. Jukes · Kwing-So Choi · Jin-Jun Wang**

Received: 22 August 2011 / Revised: 25 December 2011 / Accepted: 7 January 2012 / Published online: 15 February 2012


**Abstract** Flow control study of a NACA 0012 airfoil with a Gurney flap was carried out in a wind tunnel, where it was demonstrated that a dielectric-barrier-discharge (DBD) plasma actuator attached to the flap could increase the lift further, but with a small drag penalty. Time-resolved PIV measurements of the near-wake region indicated that the plasma forcing shifted the wake downwards, reducing its recirculation length. Analysis of wake vortex dynamics suggested that the plasma actuator initially amplified the lower wake shear layer by adding momentum along the downstream surface of the Gurney flap. This enhanced mutual entrainment between the upper and lower wake vortices, leading to an increase in lift on the airfoil.

## 1 Introduction

The dielectric-barrier-discharge (DBD) plasma actuator has received much attention over the last two decades due to its unique advantages over traditional actuators. It usually consists of an exposed electrode and an embedded electrode, separated by a dielectric sheet. The electrodes are energized at high voltage and frequency, causing the air over the embedded electrode to ionize which induces a wall-jet flow (Jukes et al. 2006). The DBD plasma actuator can be rapidly turned on and off as required.

The plasma actuator has been used to improve the aerodynamics of an airfoil, either by placing it near the leading edge as a separation control device (Post and Corke 2006; Sosa et al. 2007; He et al. 2009) or near the trailing edge as a plasma flap (He et al. 2009; Little et al. 2010). Both methods can result in an increase in lift coefficient. He et al. (2009) proposed a concept of "virtual section shape" using the plasma actuator, while Okita et al. (2008) used the DBD plasma actuator as a vortex generator to control flow over a NACA 0024 airfoil. More details on the DBD plasma actuator can be found elsewhere (Moreau 2007; Corke et al. 2009, 2010).

The Gurney flap is a small flat plate attached to the trailing edge on the pressure side of an airfoil, which enhances the aerodynamics performance of aircrafts, wings and high lift devices (Wang et al. 2008). Li et al. (2002, 2003), Lee and Ko (2009) and Lee (2010) applied the Gurney flap to control a NACA 0012 airfoil. They all concluded that the Gurney flap could increase the lift coefficient, where the Gurney flap increases the effective camber of the airfoil to enhance the lift performance. However, there is an inevitable drag penalty associated with this lift enhancement. Therefore, the Gurney flap would be more useful if it could be stored during cruise.

Traub et al. (2004) carried out a wind tunnel study of a NACA 0015 airfoil with a jet slot located at 2% chord upstream of the trailing edge. The jet Gurney flap with a 0.68% momentum coefficient resulted in lift and momentum increases equivalent to a 0.75% chord Gurney flap. Moreover, the power required by the jet flap was less than the power loss due to drag penalty of the conventional Gurney flap at low angles of attack. Traub and Agarwal

L.-H. Feng · J.-J. Wang
Fluid Mechanics Key Laboratory of Education Ministry, Beijing University of Aeronautics and Astronautics, Beijing 100191, China

L.-H. Feng · T. N. Jukes · K.-S. Choi (✉)
Faculty of Engineering, University of Nottingham, University Park, Nottingham NG7 2RD, UK
e-mail: kwing-so.choi@nottingham.ac.uk

T. N. Jukes
Research Centre for New Fuels and Vehicle Technology, AIST, Tsukuba 305-8564, Japan

(2008) further undertook an investigation into the Gurney flap in conjunction with a jet flap at low Reynolds numbers. They found that the jet forcing further increased the lift coefficient by the Gurney flap alone.

Recently, Zhang et al. (2009) numerically investigated the effect of a "plasma Gurney flap" on the aerodynamic characteristics of a NACA 0012 airfoil, where the plasma actuator was attached to the blunt trailing edge of the airfoil. Their results indicated that the "plasma Gurney flap" increased the lift and nose-down moment of the airfoil in a similar way to the conventional Gurney flap. It was also shown that the Kármán vortices were weakened near the trailing edge, which reduced the drag and thus increased the lift-to-drag ratio.

The aim of the present investigation is to obtain a greater lift enhancement with less drag penalty by combining a DBD plasma actuator with a Gurney flap. Here, a possibility of adopting the DBD plasma actuator to enhance the lift on a NACA 0012 airfoil was experimentally investigated by attaching it to the Gurney flap. A dynamic force balance was used to measure the lift and drag forces, while a time-resolved PIV system was employed to measure the velocity field in the near-wake region to investigate the vortex dynamics associated with the lift enhancement.

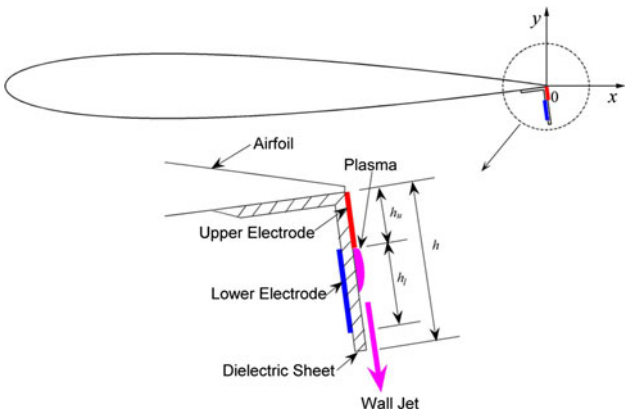


**Fig. 1** Sketch of the NACA 0012 airfoil with Gurney flap and plasma actuator

**Table 1** Parameters of Gurney flap with plasma actuator

| Gurney flap height $h$ (mm) | $h/c$ (%) | Upper electrode width $h_u$ (mm) | Lower electrode width $h_l$ (mm) | Peak-to-peak voltage $E$ ($kV_{p-p}$) | Excitation frequency $f$ (kHz) |
|---|---|---|---|---|---|
| 3.0 | 3.0 | 1.0 | 1.5 | 6.9 | 19.8 |
| 4.5 | 4.5 | 1.0 | 3.0 | 9.8 | 17.8 |
| 7.0 | 7.0 | 2.5 | 4.5 | 9.8 | 18.5 |

## 2 Experimental set-up

The experiment was conducted in a low-speed wind tunnel with a test section 1.5 m × 0.3 m × 0.3 m at the University of Nottingham. The test model used was a NACA 0012 airfoil with the chord length $c = 100$ mm and the span $b = 250$ mm, giving the aspect ratio $b/c = 2.5$. Tests were carried out at three free-stream velocities of $U_\infty = 3.0$, 4.3 and 5.3 m/s, corresponding to Reynolds numbers $Re = 20{,}000$, 28,000 and 35,000, respectively, based on the airfoil chord length. End plates of 300 mm × 200 mm in the streamwise and vertical directions were used to improve the two dimensionality of the flow field.

The Gurney flap was attached to the airfoil perpendicular to the bottom surface at the trailing edge, as shown in Fig. 1. Three different Gurney flap configurations incorporating DBD plasma actuators were tested, of height $h = 3.0$ mm (3.0%$c$), 4.5 mm (4.5%$c$) and 7.0 mm (7.0%$c$), as listed in Table 1. For the 7.0 mm Gurney flap, for example, the plasma actuator consisted of a 2.5-mm-wide upper copper electrode with a 4.5-mm-wide lower copper electrode (see Fig. 1). The thickness of both copper electrodes was 17 μm and the plasma actuator spanned the central 220 mm of the airfoil. The Gurney flap was constructed from 250-μm-thick Mylar sheet, which also served as the dielectric for the DBD actuator. The lower electrodes of plasma actuators were covered by an insulating tape to prevent plasma discharge on the upstream side of the Gurney flap. It was not possible to produce Gurney flaps less than 3.0 mm in height since an arc would occur between the upper and lower electrodes around the tip of the flap, preventing the formation of stable DBD plasma.

A two-component dynamic force balance was mounted on the side wall of the test section to measure the time history of lift and drag coefficients on the airfoil. The balance consisted of two parallelograms arranged in an "L" shape. Each parallelogram was instrumented with four strain gauges, which were wired to form two Wheatstone bridges. The bridge input voltage was supplied from two Fylde FE-379-TA transducer amplifiers, while the bridge output was recorded at 2 kHz using an IoTech 488/8SA analog to digital converter and stored on a computer. Care was taken to shield the strain gauges and transducer amplifiers from the RF noise emitted by DBD by using copper Faraday cages and shielded cables. This reduced the noise pickup to less than ±4μV (±1μN). Further details of the force balance can be found elsewhere (Jukes and Choi 2009a, b, c). The airfoil model was mounted on the force balance through a rod located at the centerline, 25%$c$ from the leading edge. Force calibration was performed by attaching precision weights to the supporting rod vertically

for lift force and horizontally via a low-friction pulley system for drag force. The accuracy of force measurements was better than ±0.01 N and the angle of attack for the airfoil could be set within ±0.25°.

Time-resolved particle image velocimetry (PIV) from Dantec Dynamics was used to measure the velocity field in the airfoil wake. This system consisted of a Phantom V12.1 high-speed camera, a Litron LDY302-PIV 100 W Nd:YLF laser, a seeding particle generator and a computer. The seeing particles used here were 1-μm-diameter droplets of olive oil. For the flow around the airfoil, the field of view was approximately 70 mm × 40 mm, with 1,280 × 800 pixels resolution in the streamwise and vertical directions, respectively. The time delay between laser pulses was typically 50–95 μs, where the timing was controlled within Dantec Dynamic Studio v3.0 and Dantec timing hardware. This typically resulted in a particle displacement of around 6 pixels in the free-stream region (about 20% of an interrogation area). The sampling frequency of the camera was 2 kHz, and 4,000 image pairs were recorded continuously for each case. This included 1 s data without plasma control and 1 s data with plasma control (1.3 and 0.7 s data, respectively, for 7.0%$c$ height Gurney flap).

Dantec Dynamic Studio v3.0 was used to calculate the velocity fields from the acquired data. The interrogation window was 32 × 32 pixels with 50% overlap in both the streamwise and vertical directions. Velocity vectors were computed using a recursive cross-correlation technique (adaptive correlation with local median filter). Vectors were validated using local and median filters by calculating the deviation from the surrounding vectors. This always resulted in less than 5% erroneous vectors, which were replaced using interpolation of the surrounding vectors. The origin of the coordinate system used here is located at the trailing edge of the airfoil at 0° angle of attack, with the $x$ and $y$ axes pointing in the streamwise and vertical directions, respectively (see Fig. 1).

The plasma actuator was driven sinusoidally at high AC voltage with high frequency using a PSI PG1040F power supply, with excitation voltage $E$ and excitation frequency $f$ as listed in Table 1. In order to quantify the plasma forcing magnitude, the induced force by each plasma actuator was calculated based on the momentum theory (Jukes and Choi 2009b). Here, a control volume of 18 mm wide at 15 mm downstream of the upper electrode edge was chosen in quiescent air. The thrust per unit width is equal to the total momentum flux across this volume. Therefore, the plasma-induced force can be calculated by integrating the velocity. Figure 2 shows the change in the momentum flux $M$ with time, which quickly settles to a quasi-steady value after 0.2–0.3 s. The initial overshoot is due to the formation of the starting vortex (Jukes et al. 2008). It is shown that the 7.0%$c$ plasma actuator induced the greatest momentum flux, while the 3.0%$c$ plasma actuator had the smallest due to the difference in $E$.

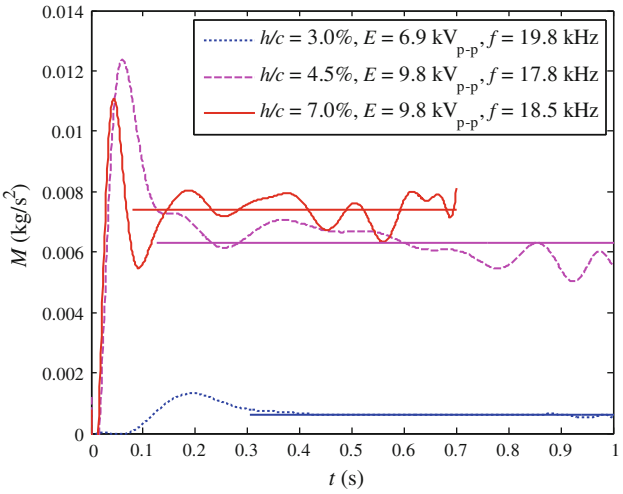


**Fig. 2** Momentum flux induced by the plasma actuator. The *straight lines* denote the mean momentum flux $M_m$ for each case

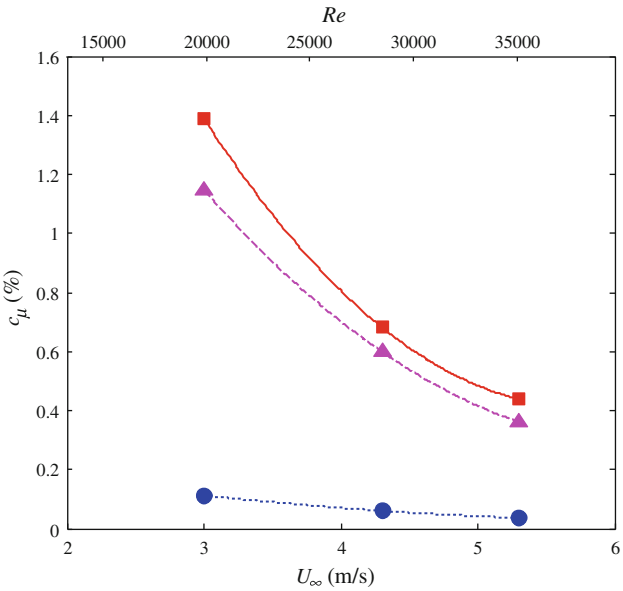


**Fig. 3** Momentum coefficient for all experimental cases. *Filled circle*, $h/c = 3.0\%$; *filled triangle*, $h/c = 4.5\%$; *filled square*, $h/c = 7.0\%$. The *dotted*, *dashed* and *solid lines* show the fitting curves for these three cases

The momentum coefficient of plasma jet, as defined by $C_\mu = 2M_m/\rho U_\infty^2$, is given in Fig. 3. This shows that the momentum coefficient $C_\mu$ takes a value between 0.04 and 1.39%, where the largest momentum coefficient is provided by the 7.0%$c$ plasma actuator.

## 3 Results and analysis

### 3.1 Aerodynamic forces

The instantaneous lift and drag coefficients obtained from dynamic force balance measurements are shown in Fig. 4 as an example to show the control effect of plasma forcing. When the plasma actuator is turned on, both the lift and drag coefficients are increased by about 35 and 30%, respectively.

Figure 5 shows the time-averaged lift and drag coefficients of a NACA 0012 airfoil versus angle of attack $\alpha$ at $Re = 20{,}000$, showing that the lift coefficient is increased with an increase in the Gurney flap height. When the plasma actuator is turned on, the lift coefficient is increased for the entire angles of attack tested here. The plasma forcing with $C_\mu = 1.15\%$ on a 4.5%$c$ Gurney flap seems to achieve a lift coefficient comparable to a 7.0%$c$ Gurney flap without plasma control. The plasma forcing with $C_\mu = 1.39\%$ on a 7.0%$c$ Gurney flap shifts the lift coefficient upwards by about 0.15 for the entire angles of attack. Therefore, the DBD plasma actuator on the Gurney flap acts to increase the equivalent flap height. However, the drag coefficient also increases with the Gurney flap height (Fig. 5b). The additional lift produced by the present plasma forcing is similar to the results by the jet flap (Traub et al. 2004; Traub and Agarwal 2008), the plasma flap (He et al. 2009) and the plasma Gurney flap (Zhang et al. 2009).

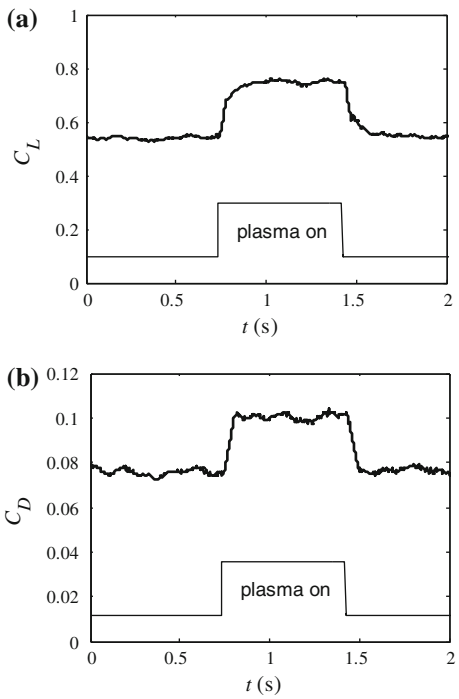


**Fig. 4** Time evolution of lift coefficient (**a**) and drag coefficient (**b**) for $\alpha = 0°$, $h/c = 7.0\%$, $Re = 20{,}000$, $C_\mu = 1.39\%$. The pulse signal (*thin line*) represents the excitation signal for the plasma actuator, which is turned on when the pulse appears

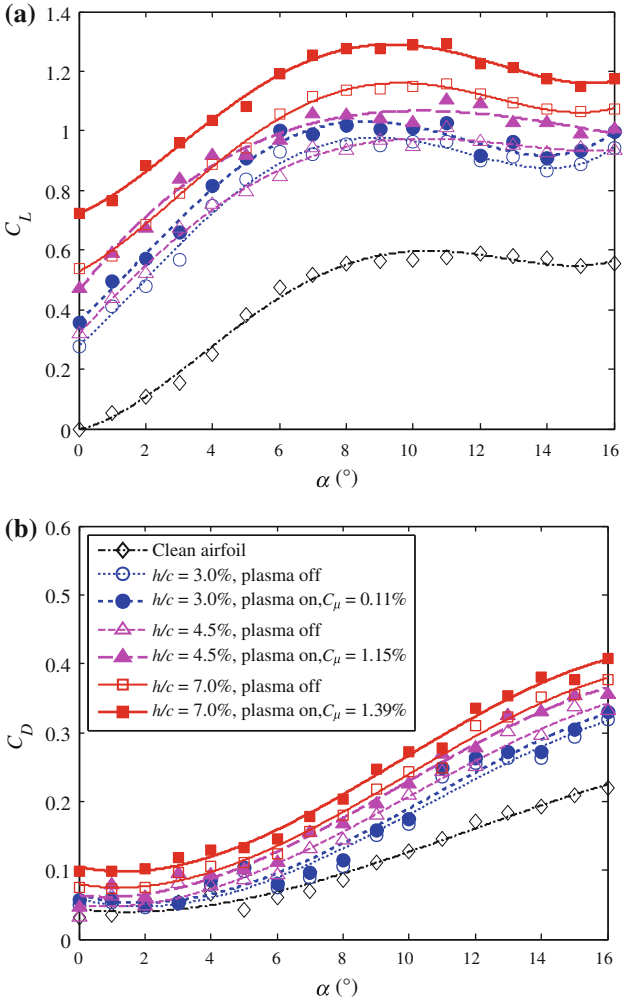


**Fig. 5** Lift coefficient (**a**) and drag coefficient (**b**) versus angle of attack at $Re = 20{,}000$

Based on thin-airfoil theory, Liu and Montefort (2007) proposed that the lift coefficient increments $\Delta C_L$ by Gurney flaps should be proportional to the square root of the flap height. On the other hand, the drag coefficient increments $\Delta C_D$ by Gurney flaps should be linearly proportional to the flap height (Greenblatt 2011). These predictions were confirmed by Bechert et al. (2000) and Yu et al. (2011), who carried out wind tunnel tests and numerical simulations of Gurney flaps, respectively. Figure 6a compares the present data on NACA 0012 to show $\Delta C_L$ as a function of $h/c$ at zero angle of attack, indicating that the lift increments by Gurney flaps is given by $\Delta C_L = 1.5\sqrt{h/c}$. Also shown in Fig. 6a are the data obtained by Bechert et al. (2000) on an HQ17 airfoil, which can be represented by $\Delta C_L = 3.2\sqrt{h/c}$. The difference in the proportionality constant is due to the difference in the airfoil type as well

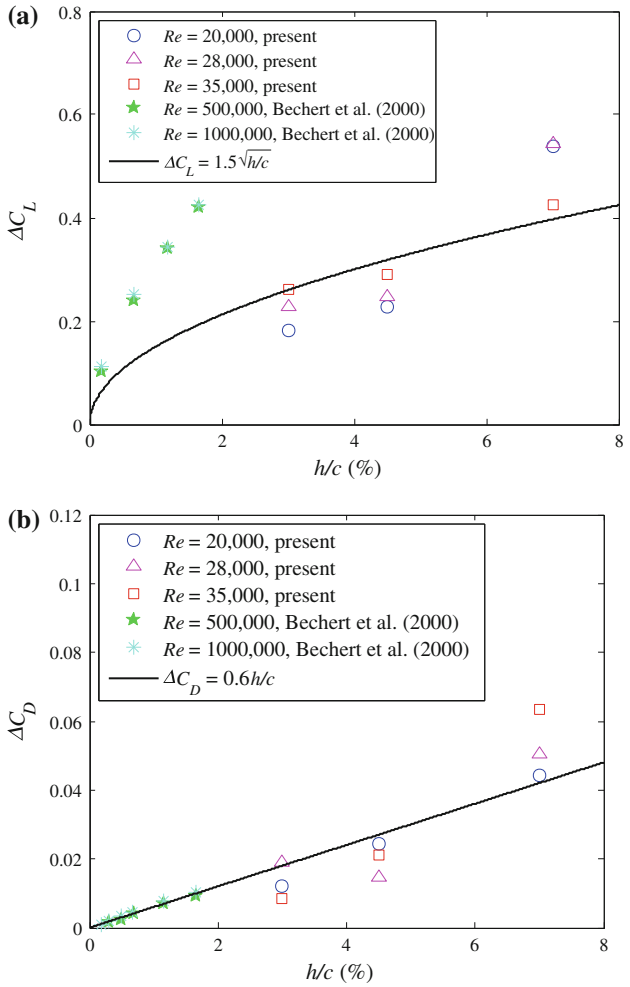


**Fig. 6** Increment of the lift coefficient (**a**) and drag coefficient (**b**) in comparison with the clean airfoil as a function of the Gurney flap height $h/c$ at $\alpha = 0°$

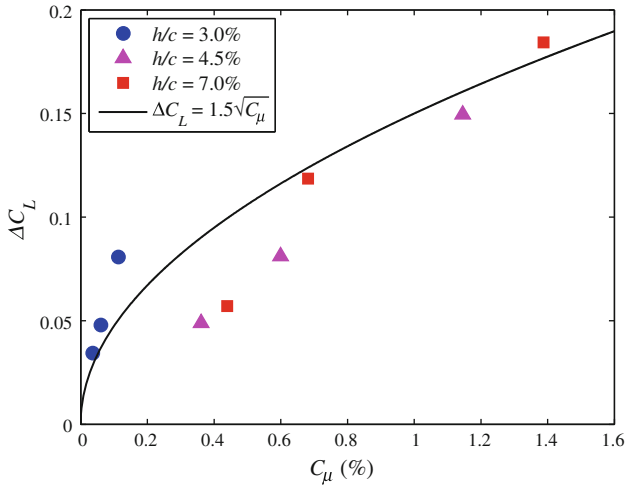


**Fig. 7** Lift coefficient increment by plasma actuator at $\alpha = 0°$ as a function of the plasma jet moment coefficient $C_\mu$

as the Reynolds number (Greenblatt 2011). The drag increments $\Delta C_D$ by Gurney flaps at zero angle of attack are shown in Fig. 6b as a function of $h/c$, suggesting that a linear relationship given by $\Delta C_D = 0.6\,(h/c)$ is valid for a wide range of the Reynolds number ($Re = 20{,}000$–$1000{,}000$) and the non-dimensional flap height ($h/c \leq 7.0\%$), even for different airfoil types.

The lift coefficient increment $\Delta C_L$ by plasma forcing is shown in Fig. 7 as a function of the plasma momentum coefficient $C_\mu$, indicating that the relationship can be represented by $\Delta C_L = 1.5\sqrt{C_\mu}$. This has a good agreement with the theoretical prediction for a jet flap by Siestrunck (1961), suggesting that the mechanism of lift increment by plasma forcing over a Gurney flap is similar to that of jet flap. A comparison of data given in Figs. 6a and 7 suggests that the plasma forcing with $C_\mu = 1\%$ has an effective Gurney flap height increment equivalent to $h/c = 1\%$.

### 3.2 Characteristics of the wake

Figure 8 shows the time-averaged velocity distribution in the near-wake region of the Gurney flap without and with plasma control for $\alpha = 2°$, $h/c = 7.0\%$, $Re = 20{,}000$, $C_\mu = 1.39\%$. Time averaging was performed over 2,200 and 1,400 instantaneous snapshots for plasma-off and plasma-on cases, respectively. Figure 8 indicates that additional plasma forcing makes the recirculation length behind the Gurney flap much shorter. Here, the recirculation length, $l_r$, was measured as the distance from the Gurney flap to the saddle point, as shown in Fig. 8c, d, which is summarized in Fig. 9. This figure clearly shows that the recirculation length is reduced by plasma forcing, where the reduction becomes greater with an increase in the pre-stall angle of attack. Zhang et al. (2009) and Little et al. (2010) also observed a reduction in the length of recirculation region by the plasma Gurney flap and the plasma flap, respectively.

The time-averaged streamwise velocity distribution in a wake is shown in Fig. 10. This indicates that Gurney flap control turns the wake downwards, which is much greater with additional plasma control. According to Lee and Ko (2009), the downward turning of the near wake increases the suction pressure over the Gurney flap, leading to an increase in the lift coefficient of the airfoil. It should be noted that there is a greater velocity defect in the wake, therefore, a greater drag with the Gurney flap and plasma control. However, as shown in Fig. 10, the velocity defect recovers rapidly with additional plasma forcing.

Figure 11 shows the distribution of turbulent kinetic energy behind the 7%$c$ Gurney flap without and with plasma at $\alpha = 2°$. This shows that the turbulent kinetic energy in a near-wake region is increased by plasma forcing, where the energy peak is moved much closer to the

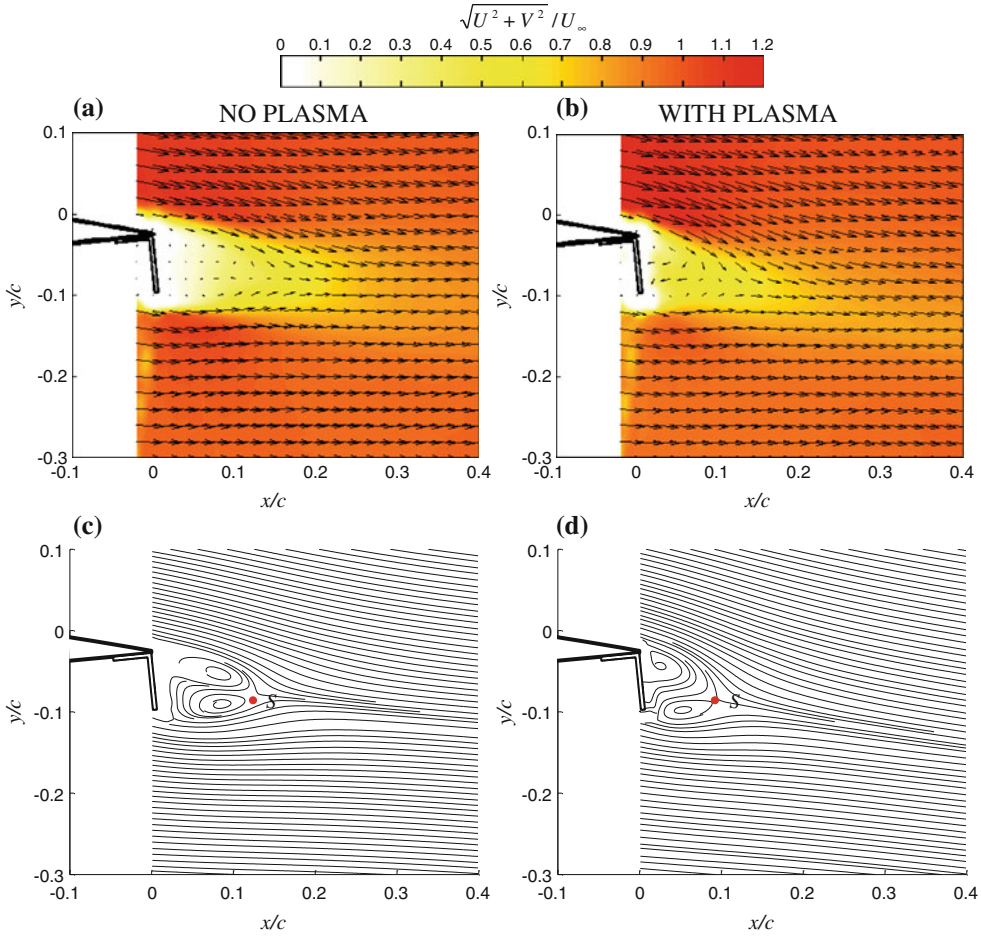


**Fig. 8** Time-averaged velocity $\sqrt{U^2+V^2}/U_\infty$ superposed with velocity vector (**a**, **b**) and streamline (**c**, **d**), for the airfoil installed Gurney flap without plasma control (*left column*) and with plasma control (*right column*) at $\alpha = 2°$, $h/c = 7.0\%$, $Re = 20{,}000$, $C_\mu = 1.39\%$

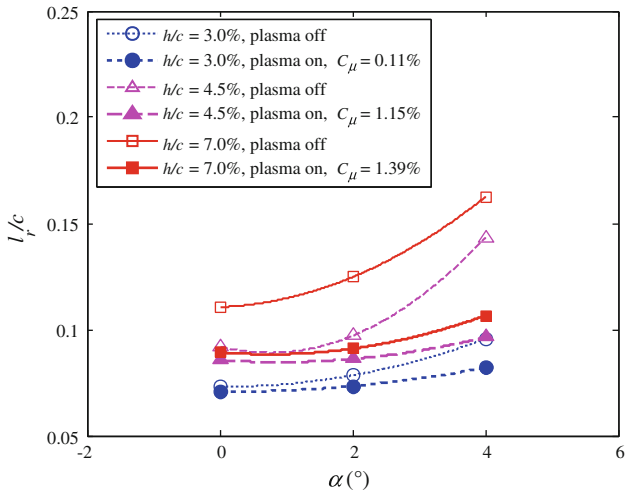


**Fig. 9** Summary of the recirculation length versus angle of attack at $Re = 20{,}000$

Gurney flap. However, the turbulent kinetic energy quickly reduces in the downstream, reflecting an initial increase in the velocity deficit, followed by a reduction in downstream (see Fig. 10). The wake vortex dynamics of near-wake region to bring these changes in turbulent kinetic energy will be discussed further in Sect. 3.3.

Figure 12 shows the streamwise distribution of the wake half-width $b_{1/2}$ obtained from the velocity deficit profiles given in Fig. 10. Here, the wake half-width is defined as the distance across the wake at which the velocity defect becomes a half of its maximum value. It is shown that the minimum wake width position is shifted closer to the Gurney flap by the DBD plasma actuator. Here, the minimum half-width location corresponds to the end of the recirculation region. Our results, therefore, suggest that the recirculation region becomes much shorter and narrower with additional plasma forcing on the Gurney flap.

Using a technique developed by von Ellenrieder and Pothos (2008) and Godoy-Diana et al. (2009), the wake deflection angle $\theta$ between the free-stream direction and the line of minimum mean streamwise velocity (the maximum defect velocity) is obtained, as shown in Fig. 13. These results are summarized in Fig. 14, showing that the airfoil wake is shifted downwards by plasma forcing by up to $\Delta\theta = 3°$.

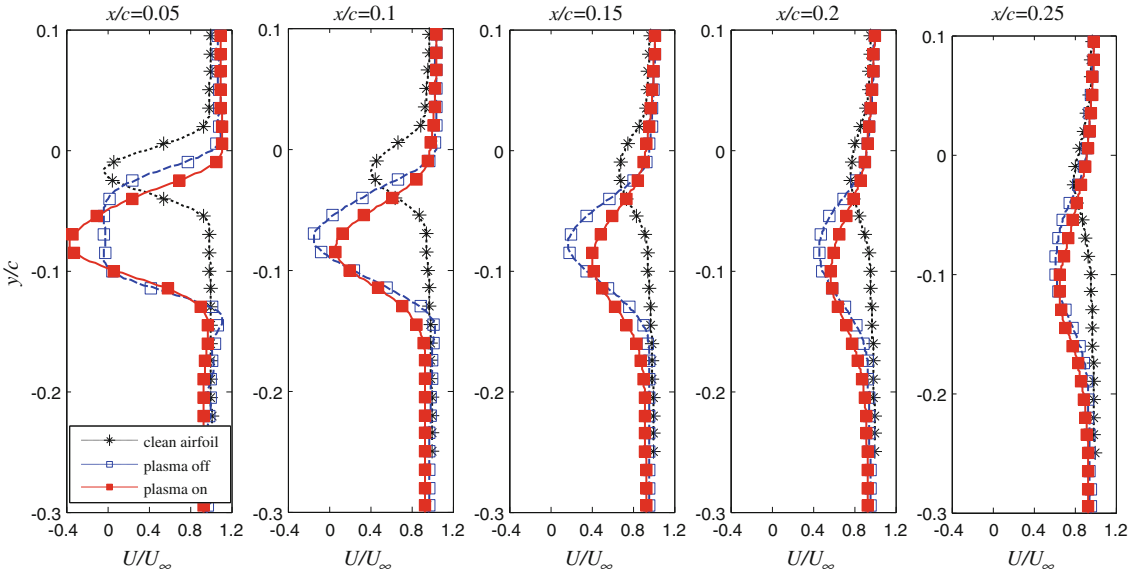


**Fig. 10** Vertical distribution of the time-averaged streamwise velocity at angle of attack $\alpha = 2°$ for the clean airfoil at $Re = 35{,}000$ and the $h/c = 7.0\%$ Gurney flap without and with plasma control ($C_\mu = 1.39\%$) at $Re = 20{,}000$

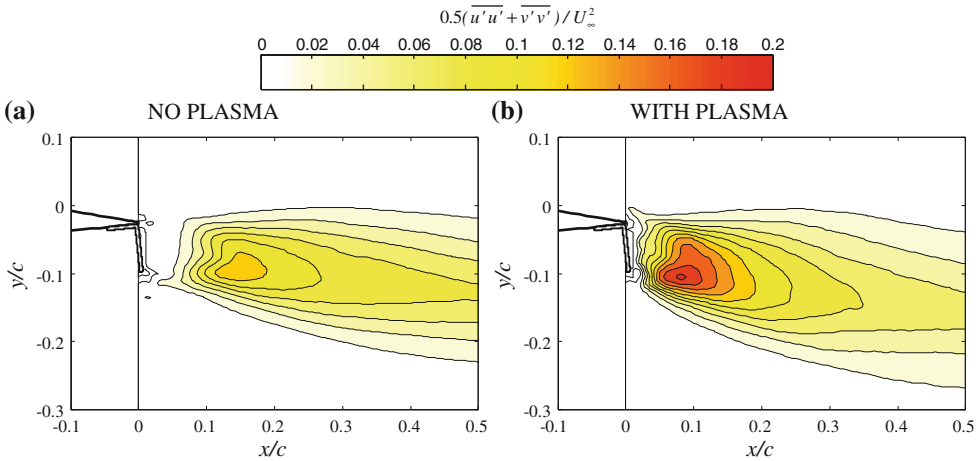


**Fig. 11** Distribution of the turbulent kinetic energy $0.5(\overline{u'u'} + \overline{v'v'})/U_\infty^2$ for the Gurney flap without (**a**) and with (**b**) plasma control at $\alpha = 2°$, $h/c = 7.0\%$, $Re = 20{,}000$, $C_\mu = 1.39\%$

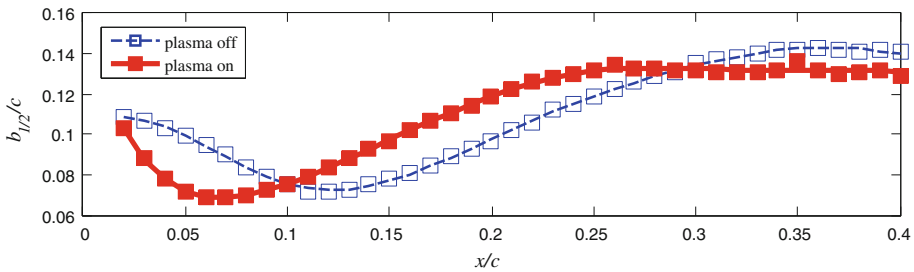


**Fig. 12** Streamwise distribution of the airfoil wake half-width for the Gurney flap without and with plasma control at $\alpha = 2°$, $h/c = 7.0\%$, $Re = 20{,}000$, $C_\mu = 1.39\%$

### 3.3 Wake vortex dynamics

The Gurney flap decreases the dominant shedding frequency of the wake vortex. This reduction becomes even greater when the plasma forcing is applied. The result for $\alpha = 2°$, $Re = 35{,}000$ is shown in Fig. 15, depicting that the dominant shedding frequency is reduced by about 27 and 32% by the Gurney flap without and with plasma forcing, respectively. It is worth noting, however, that the dominant shedding frequency does not change within a

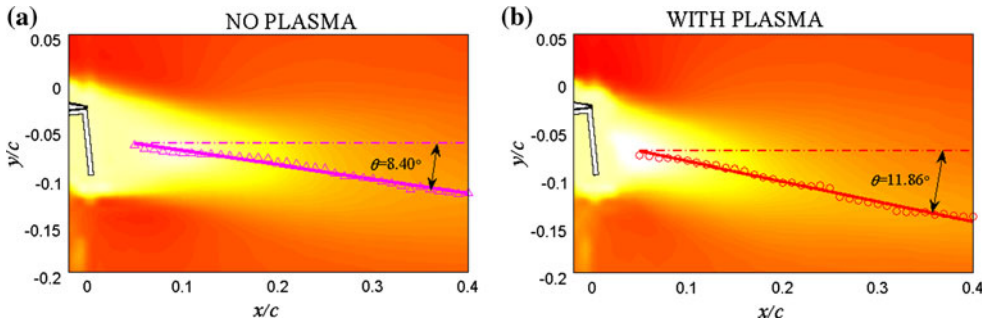


**Fig. 13** Detection of the wake deflection angle for the cases of airfoil controlled by Gurney flap without (**a**) and with (**b**) plasma control at $\alpha = 2°$, $h/c = 7.0\%$, $Re = 20{,}000$, $C_\mu = 1.39\%$

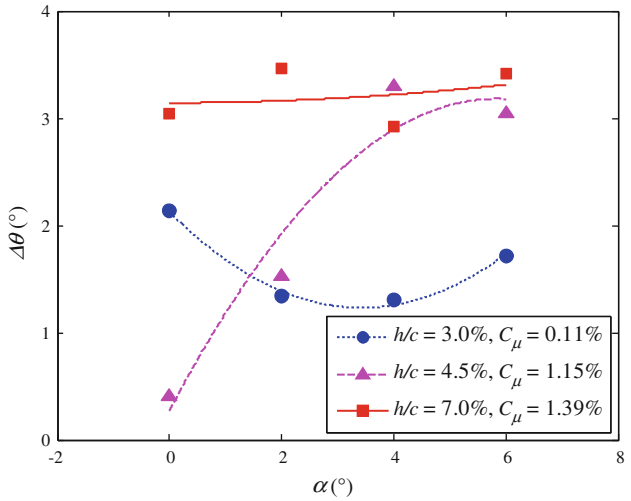


**Fig. 14** Difference of wake deflection angle between plasma on and plasma off versus angle of attack at $Re = 20{,}000$

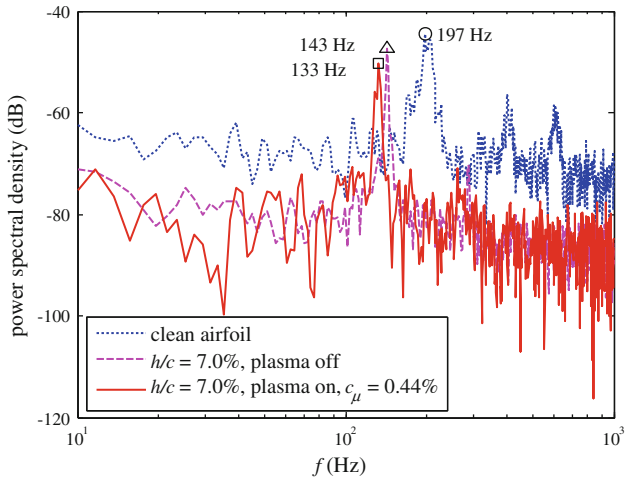


**Fig. 15** Power spectral density (PSD) analysis of the spanwise vorticity $\omega_z c/U_\infty$ from PIV data at $x/c = 0.15$, $y/c = 0$, $\alpha = 2°$, $Re = 35{,}000$

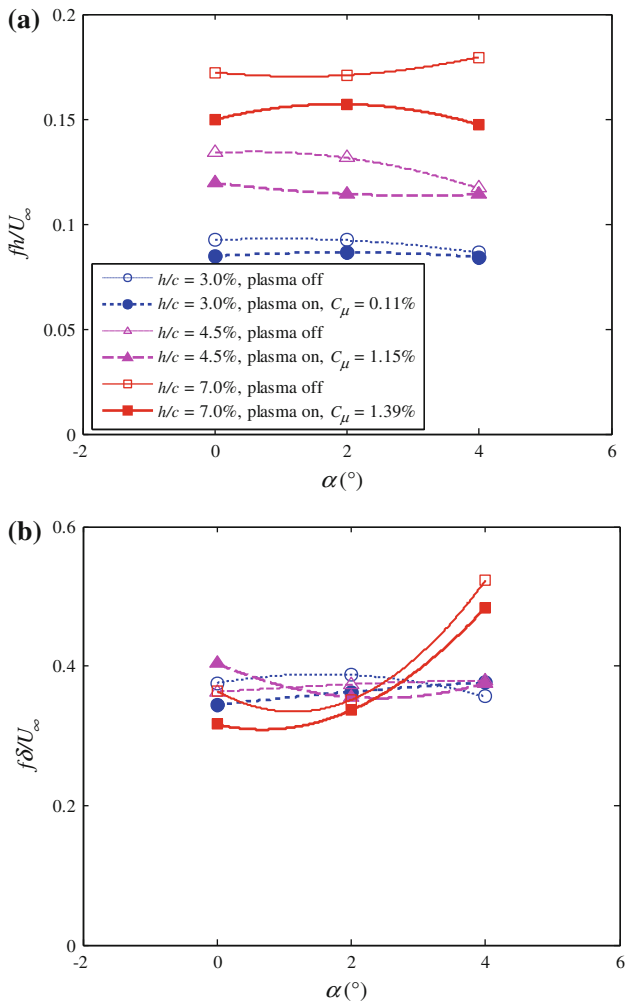


**Fig. 16** Variations of the dominant wake vortex shedding frequency $fh/U_\infty$ (**a**) and $f\delta/U_\infty$ (**b**) versus angle of attack at $Re = 20{,}000$, where $\delta$ is the distance between upper and lower boundary layers measured at $0.015c$ downstream of the airfoil trailing edge

near-wake region. The reduction in the power spectrum peak indicates that there might be a possible noise reduction by the plasma control (Kuo and Sarigul-Klijn 2010).

The Gurney flap increases the dimensionless frequency $fh/U_\infty$, while the additional plasma forcing seems to decrease the shedding frequency for $\alpha \leq 4°$, as shown in Fig. 16a. Lee and Ko (2009) suggested that the reduction in shedding frequency with an increase in the flap height was due to the increased distance between the two separating

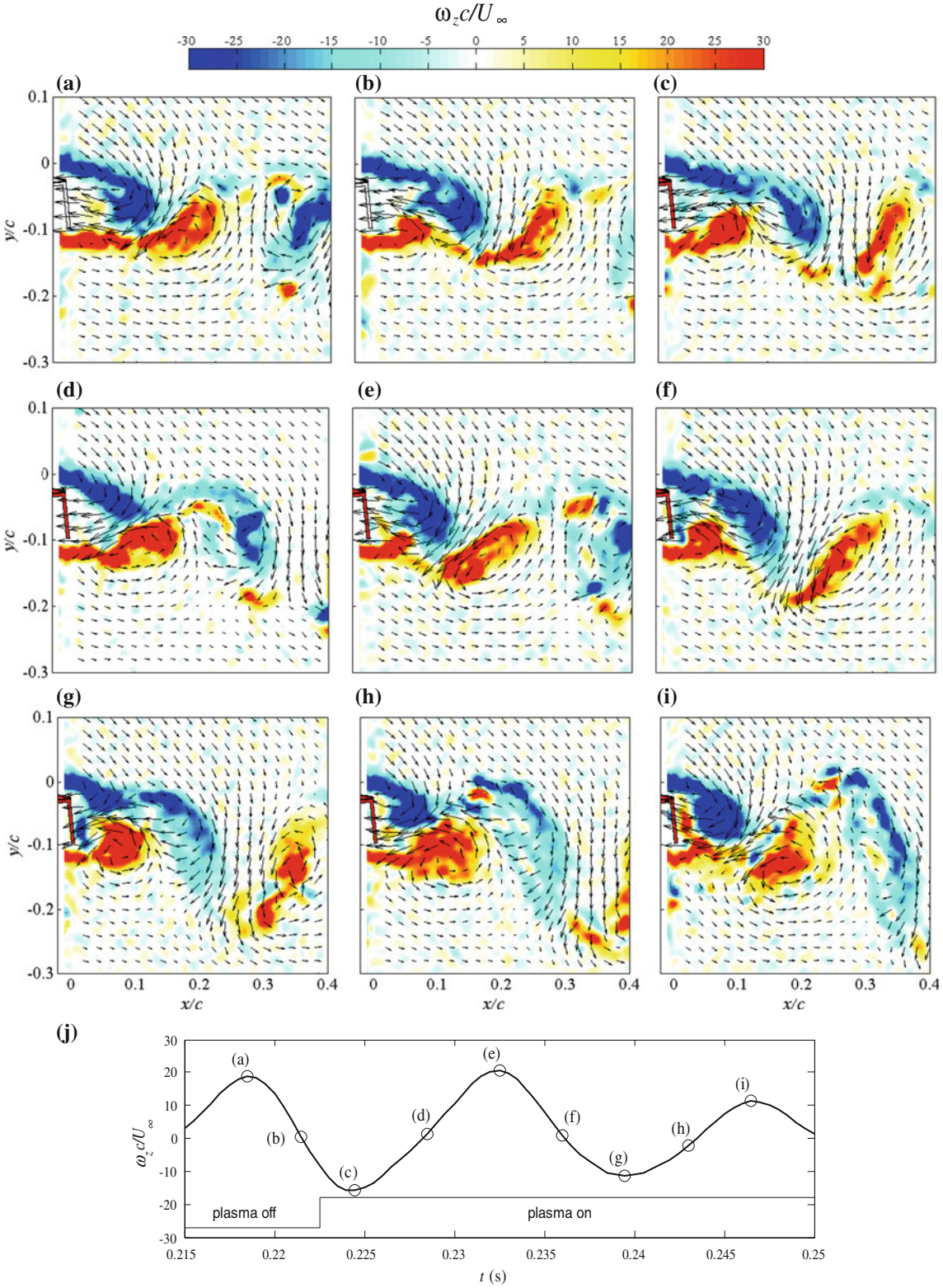


**Fig. 17** Evolution of the instantaneous spanwise vorticity field $\omega_z c/U_\infty$ superposed with velocity vector (with $0.8U_\infty$ subtracted from streamwise velocity) showing the control process of the plasma actuator from **a** to **i**, and the time history of the spanwise vorticity **j** at $x/c = 0.2$, $y/c = -0.1$ showing the selection of different phases. Control parameters: $\alpha = 2°$, $h/c = 7.0\%$, $Re = 20{,}000$, $C_\mu = 1.39\%$

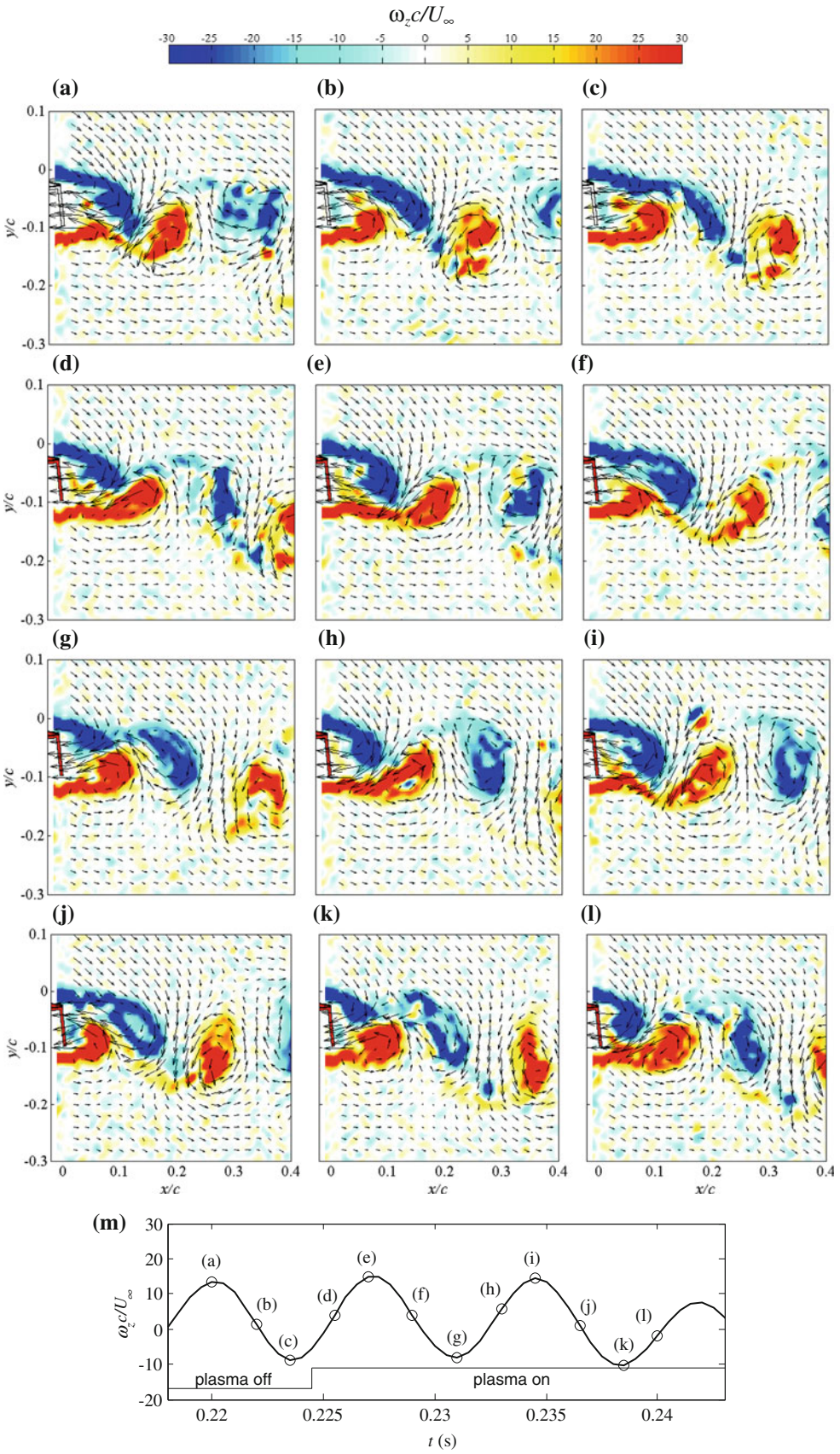


**Fig. 18** Evolution of the instantaneous spanwise vorticity field $\omega_z c/U_\infty$ superposed with velocity vector (with $0.8U_\infty$ subtracted from streamwise velocity) showing the control process of the plasma actuator from **a** to **l**, and the time history of the spanwise vorticity **m** at $x/c = 0.2$, $y/c = -0.1$ showing the selection of different phases. Control parameters: $\alpha = 2°$, $h/c = 7.0\%$, $Re = 35{,}000$, $C_\mu = 0.44\%$

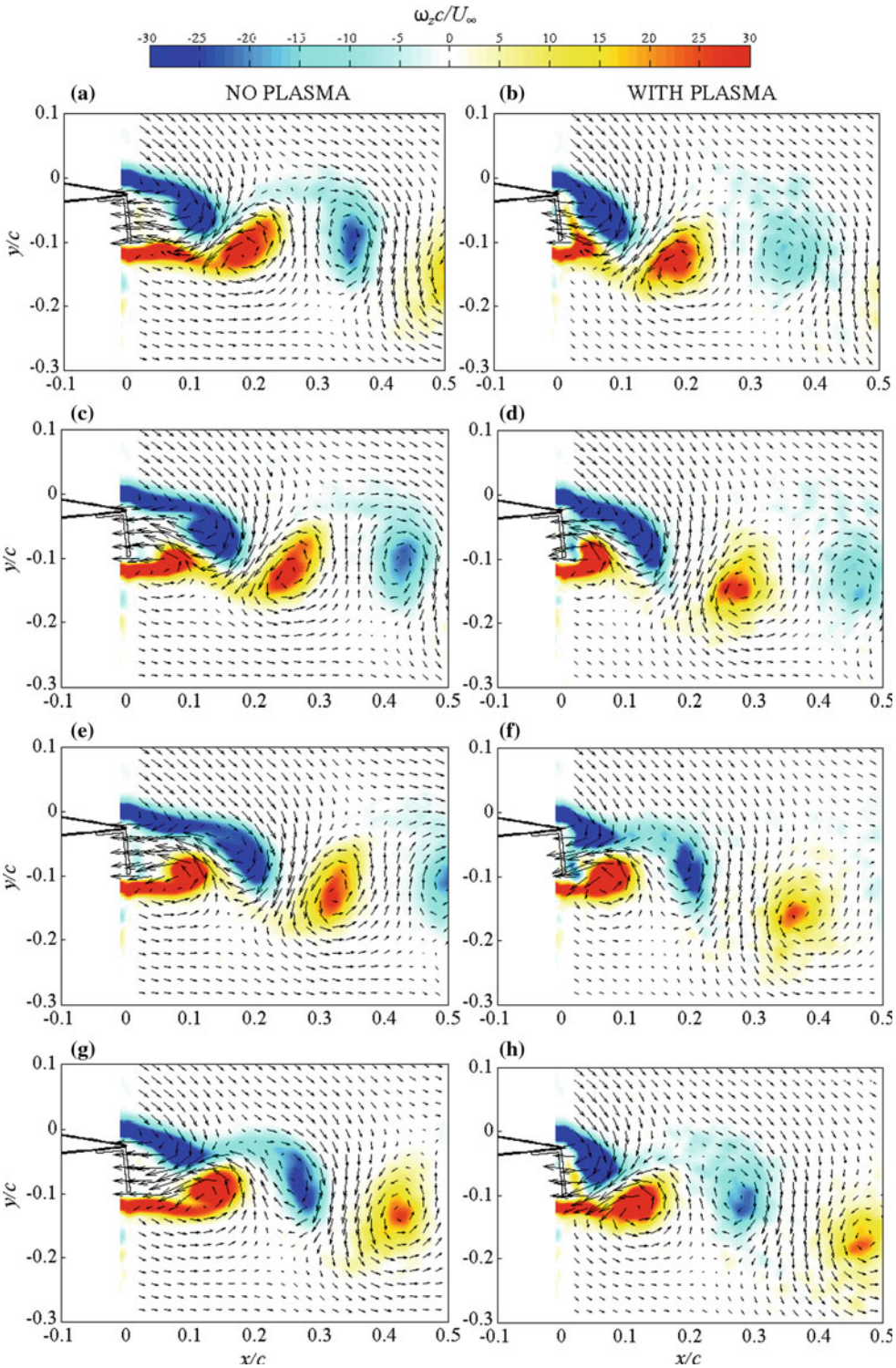


**Fig. 19** Evolution of the phase-averaged spanwise vorticity field $\omega_z c/U_\infty$ superposed with velocity vector (with $0.8U_\infty$ subtracted from streamwise velocity) at four phases 0 (**a**, **b**), $0.5\pi$ (**c**, **d**), $\pi$ (**e**, **f**) and $1.5\pi$ (**g**, **h**) for the airfoil installed Gurney flap without plasma control (*left column*) and with plasma control (*right column*) at $\alpha = 2°$, $h/c = 7.0\%$, $Re = 20{,}000$, $C_\mu = 1.39\%$

shear layers, requiring more time for the opposite shear layer to cross the wake. It has been shown by Yarusevych et al. (2009) that the variation of non-dimensional shedding frequency of a NACA 0025 airfoil can be dramatically reduced when the lateral distance $\delta$ between upper and lower shear layers is used for the length scale. Accordingly, we defined the Strouhal number by $f\delta/U_\infty$ to show the non-dimensional shedding frequency as a function of the angle of attack in Fig. 16b. It shows that the variation of frequency is indeed reduced to give $f\delta/U_\infty \approx 0.35$ as compared to the scaling based on the flap height, $fh/U_\infty$ (see Fig. 16a). Anomalous data at $\alpha = 4°$ for the 7.0%$c$ Gurney

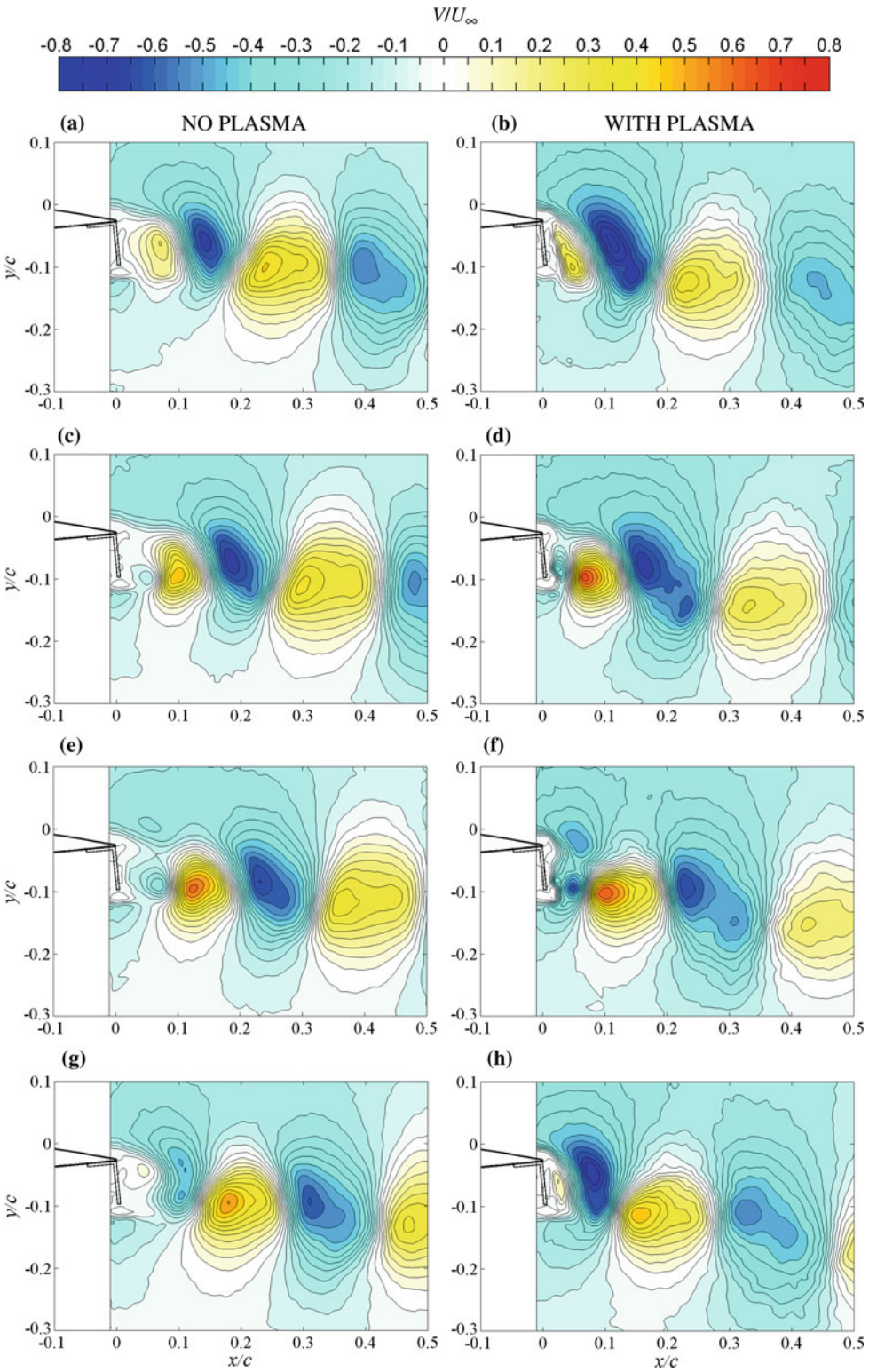


**Fig. 20** Evolution of the phase-averaged vertical velocity field $V/U_\infty$ at four phases 0 (**a**, **b**), $0.5\pi$ (**c**, **d**), $\pi$ (**e**, **f**) and $1.5\pi$ (**g**, **h**) for the airfoil installed Gurney flap without plasma control (*left column*) and with plasma control (*right column*) at $\alpha = 2°$, $h/c = 7.0\%$, $Re = 20{,}000$, $C_\mu = 1.39\%$

flap are believed to be due to a greater uncertainty involved in determining $\delta$ as the field of view for PIV measurements is limited.

Figure 17a–i shows an evolution of spanwise vorticity for $\alpha = 2°$, $h/c = 7.0\%$, $Re = 20{,}000$, $C_\mu = 1.39\%$. The phase angle of shedding vortices is indicated in Fig. 17j based on the spanwise vorticity at $x/c = 0.2$, $y/c = -0.1$. Figure 17a, b show the formation and detachment of the vortex from the lower shear layer before the plasma forcing is applied. The wake shear layers interact with each other

by drawing fluid from the opposite side of the Gurney flap across the wake, thus forming alternating vortex shedding downstream. This is similar to the Kármán vortex street from a circular cylinder (Gerrard 1966; Cantwell and Coles 1983).

When the plasma is actuated (from Fig. 17c forward, as indicated by the red Gurney flap in this and subsequent plots), the momentum is added to the lower shear layer from the downstream side of the Gurney flap, leading to a stronger vortex on this side. Thus, the vortex grows quicker and it reaches across the wake faster to entrain the shear layer from the opposite side of the airfoil. Therefore, the upper wake vortex is enhanced by the entrainment effect of the stronger lower wake vortex. During its formation process, the upper vortex also entrains the lower wake shear layer across the wake close to the Gurney flap (Fig. 17i). This leads to a shorter vortex formation length. Such process is very similar to that observed around a circular cylinder under plasma actuator control, as described by Jukes and Choi (2009b).

It was observed that no matter when the plasma actuator turned on, the lower shear layer was always magnified first. This is followed by the enhanced mutual entrainment between the upper and lower wake vortices. Figure 18 shows a sequence of vortical flow in the near-wake region, where the plasma actuator is turned on as the upper wake vortex is detaching from the shear layer. This is the opposite case to that in Fig. 17, showing a similar control process as mentioned above, although it takes two extra periods before the lower wake vortex is magnified.

For a better understanding of the variations of the flow field induced by the plasma forcing, phase-averaged results based on PIV measurements are given in Figs. 19 and 20. The technique used here to determine the phase angle was similar to that of Kim et al. (2006) and Zhou and Yiu (2006). Here, the spanwise vorticity at $x/c = 0.2$, $y/c = -0.1$ was used as a reference signal. Phase average was performed over 78 and 45 cycles for plasma-off and plasma-on cases, respectively.

Figure 19 shows the phase-averaged spanwise vorticity field for $\alpha = 2°$, $h/c = 7.0\%$, $Re = 20{,}000$, $C_\mu = 1.39\%$. The enhanced entrainment effect due to additional plasma forcing between the upper and lower wake vortices can be clearly seen here. For example in Fig. 19a, b, the vortex on the upper shear layer has just reached the shear layer on the lower surface so that the vortex formation process of the lower vortex is about to start. With plasma, the lower vortex develops stronger and closer to the downstream side of the Gurney flap (see Fig. 19c, d). The effect of added momentum is especially evident in Fig. 19e, f, where the entrainment of the upper vortex has occurred more rapidly due to the enhanced lower shear layer. Here, it can also be seen that the upper shear layer has been entrained toward the DBD plasma actuator on the Gurney flap. This may be due to the suction effect of the actuator as it accelerates fluid in the negative $y$-direction (downwards). In fact the upper shear layer appears to change its direction sharply, diverting vertically down along the Gurney flap rear surface (see Fig. 19f at $x/c = 0$, $-0.1 \leq y/c \leq 0$). As a result, the vortex formation length is reduced from $0.12c$ to $0.06c$, based on the position of the maximum streamwise velocity fluctuation (Zdravkovich 1997).

The velocity field in the near-wake region is also changed by the additional plasma forcing. This is shown in Fig. 20, where the vertical velocity magnitude is increased by plasma control. This explains a reduction in the vortex formation length behind the Gurney flap. Troolin et al. (2006) have pointed that such increase in the net negative vertical velocity on the airfoil wake leads to an enhancement of circulation and thus the lift force.

## 4 Conclusions

Flow control around a NACA 0012 airfoil by the DBD plasma actuator on a Gurney flap has been investigated. A dynamic force balance and time-resolved PIV were used to measure the lift and drag coefficients and to study the velocity and vorticity fields. The present results showed that both lift and drag coefficients were increased when the plasma actuator was turned on. They also indicated that an additional plasma forcing on the Gurney flap with a jet momentum coefficient $C_\mu = 1\%$ has an effective increment in the flap height equivalent to $h/c = 1\%$.

The Gurney flap reduced the dominant shedding frequency of the wake vortex and its power spectral peak. These reductions became even greater when the plasma forcing was applied. The velocity distribution in the near-wake region indicated that the Gurney flap turned the wake downwards, and this turning became much greater with additional plasma control. This can be interpreted as an increase in the suction pressure over the Gurney flap, thereby increasing the lift coefficient of the airfoil. The recirculation region behind the Gurney flap became shorter and narrower with the plasma forcing, leading to a stronger vortex on this side. Thus, the vortex can reach across the wake faster to entrain the shear layer from the opposite side of the airfoil. It has been observed that no matter when the plasma actuator is turned on it is always the lower shear layer that was magnified first by plasma. It was also found that the negative vertical velocity on the airfoil wake was increased by plasma control, leading to an enhancement of circulation and thus the lift force.

**Acknowledgments** Financial support to carry out this joint research was provided by the China Scholarship Council and the Faculty of Engineering of the University of Nottingham.

## References

Bechert DW, Meyer R, Hage W (2000) Drag reduction of airfoils with miniflaps. Can we learn from dragonflies? In: Fluids 2000 conference and exhibit, Denver, CO, June 19–22, AIAA 2000–2315

Cantwell B, Coles D (1983) An experimental study of entrainment and transport in the turbulent near wake of a circular cylinder. J Fluid Mech 136:321–374

Corke TC, Post ML, Orlov DM (2009) Single dielectric barrier discharge plasma enhanced aerodynamics: physics, modeling and applications. Exp Fluids 46(1):1–26

Corke TC, Enloe CL, Wilkinson SP (2010) Dielectric barrier discharge plasma actuators for flow control. Annu Rev Fluid Mech 42:505–529

Gerrard JH (1966) The mechanics of the formation region of vortices behind bluff bodies. J Fluid Mech 25:401–413

Godoy-Diana R, Marais C, Aider JL, Wesfreid JE (2009) A model for the symmetry breaking of the reverse Bénard–von Kármán vortex street produced by a flapping foil. J Fluid Mech 622:23–32

Greenblatt D (2011) Application of large Gurney flaps on low Reynolds number fan blades. J Fluids Eng 133:021102

He C, Corke TC, Patel MP (2009) Plasma flaps and slats: an application of weakly ionized plasma actuators. J Aircr 46(3):864–873

Jukes TN, Choi K-S (2009a) Long lasting modifications to vortex shedding using a short plasma excitation. Phys Rev Lett 102(25):254501

Jukes TN, Choi K-S (2009b) Flow control around a circular cylinder using pulsed dielectric barrierdischarge surface plasma. Phys Fluids 21(8):084103

Jukes TN, Choi K-S (2009c) Control of unsteady flow separation over a circular cylinder using dielectric-barrier-discharge surface plasma. Phys Fluids 21(9):094106

Jukes TN, Choi K-S, Johnson GA, Scott SJ (2006) Characterization of surface plasma-induced wall flows through velocity and temperature measurements. AIAA J 44(4):764–771

Jukes TN, Choi K-S, Segawa T, Yoshida H (2008) Jet flow induced by a surface plasma actuator. Proc Inst Mech Eng Part I J Syst Control Eng 222:347–356

Kim W, Yoo JY, Sung J (2006) Dynamics of vortex lock-on in a perturbed cylinder wake. Phys Fluids 18(7):074103

Kuo BC, Sarigul-Klijn N (2010) Conceptual study of micro-tab device in airframe noise reduction: (I) 2D computation. Aerosp Sci Technol 14(5):307–315

Lee T (2010) PIV study of near-field tip vortex behind perforated Gurney flaps. Exp Fluids 50(2):351–361

Lee T, Ko LS (2009) PIV investigation of flowfield behind perforated Gurney-type flaps. Exp Fluids 46(6):1005–1019

Li YC, Wang JJ, Zhang PF (2002) Effect of Gurney flaps on a NACA0012 airfoil. Flow Turbul Combust 68(1):27–39

Li YC, Wang JJ, Zhang PF (2003) Influences of mounting angles and locations on the effects of Gurney flaps. J Aircr 40(3):494–498

Little J, Nishihara M, Adamovich I, Samimy M (2010) High-lift airfoil trailing edge separation control using a single dielectric barrier discharge plasma actuator. Exp Fluids 48(3):521–537

Liu T, Montefort J (2007) Thin-airfoil theoretical interpretation for Gurney flap lift enhancement. J Aircr 44(2):667–671

Moreau E (2007) Airflow control by non-thermal plasma actuators. J Phys D Appl Phys 40(3):605–636

Okita Y, Jukes TN, Choi K-S, Nakamura K (2008) Flow reattachment over an airfoil using surface plasma actuator. In: 4th Flow control conference, Seattle, Washington, June 23–26, 2008, AIAA 2008–4203

Post ML, Corke TC (2006) Separation control using plasma actuators: dynamic stall vortex control on oscillating airfoil. AIAA J 44(12):3125–3135

Siestrunck R (1961) General theory of the jet flap in two-dimensional flow. Boundary Layer and Flow Control. vol 1. In: Lachmann GV (eds) Pergamon Press, p 342–364

Sosa R, Artana G, Moreau E, Touchard G (2007) Stall control at high angle of attack with plasma sheet actuators. Exp Fluids 42(1):143–167

Traub LW, Agarwal G (2008) Aerodynamic characteristics of a Gurney/jet flap at low Reynolds numbers. J Aircr 45(2):424–429

Traub LW, Miller A, Rediniotis O (2004) Comparisons of a Gurney and jet-flap for hinge-less control. J Aircr 41(2):420–423

Troolin DR, Longmire EK, Lai WT (2006) Time resolved PIV analysis of flow over a NACA 0015 airfoil with Gurney flap. Exp Fluids 41(2):241–254

von Ellenrieder KD, Pothos S (2008) PIV measurements of the asymmetric wake of a two dimensional heaving hydrofoil. Exp Fluids 44(5):733–745

Wang JJ, Li YC, Choi K-S (2008) Gurney flap-lift enhancement, mechanisms and applications. Prog Aerosp Sci 44:22–47

Yarusevych S, Sullivan P, Kawall JG (2009) On vortex shedding from an airfoil in low-Reynolds-number flows. J Fluid Mech 632:245–271

Yu T, Wang JJ, Zhang PF (2011) Numerical simulation of Gurney flap on RAE-2822 supercritical airfoil. J Aircr 48(5):1565–1575

Zdravkovich MM (1997) Flow around circular cylinders, vol. 1, Fundamentals. Oxford University Press, New York

Zhang PF, Liu AB, Wang JJ (2009) Aerodynamic modification of a NACA 0012 airfoil by trailing-edge plasma Gurney flap. AIAA J 47(10):2467–2474

Zhou Y, Yiu MW (2006) Flow structure, momentum and heat transport in a two-tandem-cylinder wake. J Fluid Mech 548:17–48